Chapter 2
Structure, Mechanical Properties, and Applications of Nanocrystalline Materials

2.1 Structure

Nanocrystalline (NC) materials are composed of grain cores with well-defined atomic arrangement (e.g., face center cubic, body center cubic) joined by an interphase region composed of grain boundaries and higher-order junctions (e.g., triple junctions, quadruple junctions). Early experiments on nanocrystalline materials have shown that the interphase region and particularly grain boundaries exhibit an almost grain size–independent thickness [1]. Hence, as the grain size is decreased, the volume fraction of the interphase region increases. Supposing a tetracaidecahedral grain shape, corresponding to a realistic grain shape, the following expressions of the volume fraction of interphase (e.g., grain boundaries and triple junctions), grain boundaries, and triple junctions can be derived [2].

$$f_{in} = 1 - \left[\frac{(d-w)}{w}\right]^3, f_{gb} = \frac{3w(d-w)^2}{d^3}, f_{tj} = f_{in} - f_{gb} \tag{2.1}$$

where the subscripts *in, gb,* and *tj* refer to the interphase, the grain boundaries, and the triple junctions, respectively.

Note here that early X-ray measurements estimated the volume fraction of interphase to about ~30% with a mean grain size equal to 10 nm [3]. This measure lies well within predictions presented in Fig. 2.1. It can be observed that the volume fraction of interphase increases sharply when the grain size is in the nanocrystalline range (e.g., grain diameters smaller than ~100 nm). Also, notice that the volume fraction becomes non-negligible when the grain size is smaller than ~10 nm. Hence, it is easy to comprehend the importance of the interphase region in NC materials for the material properties are directly dependent on the microstructure of the sample, which depends itself on the fabrication process.

M. Cherkaoui, L. Capolungo, *Atomistic and Continuum Modeling of Nanocrystalline Materials*, Springer Series in Materials Science 112,
DOI 10.1007/978-0-387-46771-9_2, © Springer Science+Business Media, LLC 2009

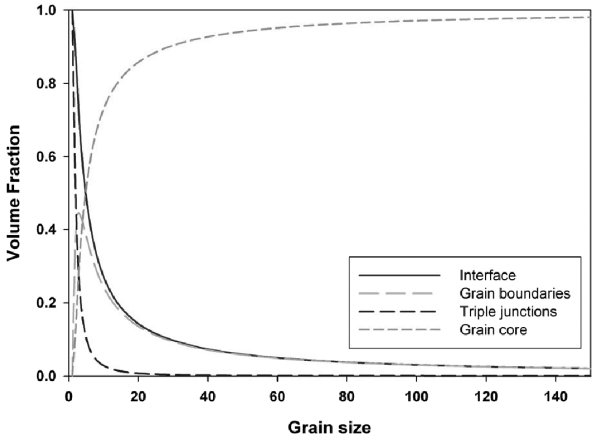

Fig. 2.1 Evolution of volume fractions of interface, grain boundaries, triple junctions, and grain cores with the grain size in nm

2.1.1 Crystallites

Independent of the fabrication process and grain size, grain cores exhibit a crystalline structure (e.g., face center cubic, body center cubic, hexagonal close packed [hcp]) up to the grain boundary. Interestingly, the lattice parameter of NC materials was reported to be size dependent. Precisely, X-ray diffraction measurements on Cu samples processed by equal channel angular pressing (ECAP) revealed that the lattice parameter within the grain cores is decreased by 0.04% [4]. It was suggested that the compressive stress imposed by none-quilibrium grain boundaries is the source of this reduced lattice parameter. The same conclusion was reached on samples fabricated by several different processes. Let us note that the lattice strain is typically more pronounced in the vicinity of grain boundaries and triple junctions.

2.1.1.1 Dislocations

Dislocation density measurements have been subject to controversial debate with reported values of dislocation density varying from $10^{15}\,m^{-2}$ to zero. Figure 2.2 presents high-resolution transmission electron microscopy (HRTEM)image of electrodeposited Ni with average grain size of ~30 nm prior to deformation [5]. The bright and dark field images (Fig. 2.2a, b) exhibit a crystalline structure devoid of dislocations and impurities indicating a low initial dislocation density within the grain cores. As shown in Fig. 2.2.c, the occasional presence of dislocation loops can be observed as well as the presence of twins. The same conclusion was also reached in the case of 20 nm grained nanocrystalline Pd processed by inert gas condensation followed by

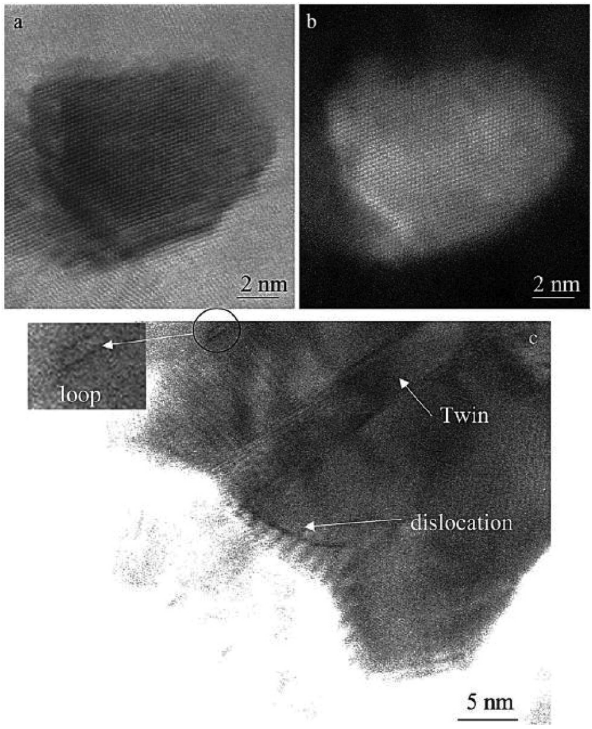

Fig. 2.2 HRTEM image of a grain core [5]

compaction [6]. However, in the case of ECAP-processed NC Cu, with grain size 150 nm, the initial dislocation density was reported in the order of $\sim 2.10^{15}\, m^{-2}$ and was about 20 times larger than that of the reference sample used the X-ray diffraction analysis [4]. A high initial dislocation density on the order of $1.10^{15}\, m^{-2}$ was also reported for nanocrystalline Ni processed by high-pressure torsion (HPT) [7]. However, let us note here that in the case of materials processed by severe plastic deformation processes, such as ECAP and HPT, grain refinement results from the large strains imposed to a coarser-grained sample. Thus, the high dislocation density measured experimentally is to be expected. Finally, let us recall that the minimum grain size achieved by severe plastic deformation is rarely smaller than ~100 nm, which falls into what is referred to as the ultrafine range, where dislocation activity is similar to that of coarser-grain materials. Finally, a dislocation density on the order of $\sim 5.10^{15}\, m^{-2}$ was reported for 15 nm grain inert gas condensation processed nanocrystalline copper [8]. Also, the same authors report average dislocation spacing close to the grain size. This signifies that a given grain will initially contain zero to 1 dislocation loop. Hence, in general, within a given grain core, the dislocation density is severely reduced compared to that of coarse-grain materials.

Consequently, dislocation activity, which is typically governed by dislocation storage and dislocation annihilation in coarse grain materials, is expected to decrease within grain cores in the case of nanocrystalline material**s.**Dislocation storage is an athermal process, corresponding to the pinning of a dislocation on a sessile obstacle (e.g., defect, stored dislocation, grain boundary), and leading to a decrease in the mean free path of mobile dislocations. Typically, strain hardening models such as the first model from Kocks and Mecking and subsequent evolutions account for the effect of grain boundaries and the effect of stored dislocations [9–12]. The effect of stored dislocations on the mobility of dislocations is accounted for via the principle of material scaling, introduced by Kuhlman Wilsdorf. Essentially, it introduces proportionality relations between the dislocations' mean free path and the dislocation density. However, so far, it has not been shown experimentally that the principle of similitude remains valid in the case of nanocrystalline materials. Dynamic recovery, which is a thermally activated mechanism, typically written with an Arrhenius type of law, is treated in phenomenological manner.

2.1.1.2 Twins

As mentioned in earlier sections, the fabrication process has great effect on the resulting microstructure. Hence, depending on the fabrication process, two NC samples with equal mean grain size can exhibit different microstructures (e.g., grain size distribution, grain boundary misorientations, impurities, pores, etc.). One of the most remarkable examples is the presence of mechanical twins in NC materials. Recall here that a twin corresponds to a mirror symmetry lattice reorientation with respect to a twinning plane. Indeed, even in face-centered cubic (FCC) metals, such as Cu and Al, which present enough slip systems (12) for dislocation glide to occur – as opposed to metals in the hcp system, in which, due to the crystal's low symmetry, twinning is a common feature of plastic deformation in coarse grain polycrystals and single crystals – twin boundaries can still be observed.

Let us note here that the presence of twins within the grain cores is directly dependent on the fabrication process. Indeed, ECAP and HPT processed nanocrystalline materials rarely exhibit the presence of twins while materials processed via inert gas condensation (IGC), electrodeposition, and mechanical alloying typically lead to the presence of twins. In Fig. 2.3 one can observe nanocrystalline Cu grain core containing a "giant step," the step is delimited by the arrowheads on the HRTEM image [13]. The stepped region is highly incoherent.

2.1.1.3 Stacking Faults

Although no quantitative data are available as to the number of stacking faults, that is the break of the sequence of close-packed planes, transmission electron microscopy (TEM)experiments and X-ray diffraction (XRD)followed by

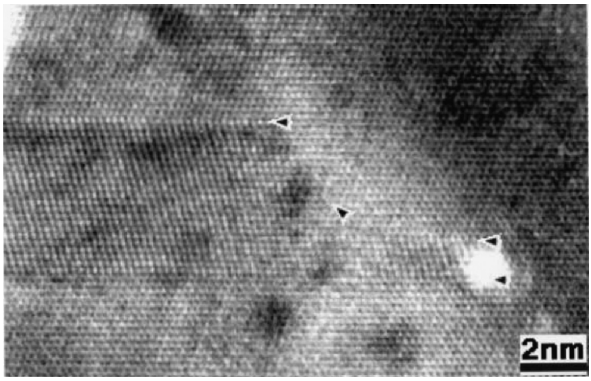

Fig. 2.3 Cu cryomilled grain core containing a stepped twin [13]

calculation of the α_{warren} probability of faults have revealed valuable information on the matter [14–17]. Calculation of the probability of faults on nanocrystalline Cu and Pd samples with grain size ranging from 5 to 25 nm and from 3 to 18 nm, respectively, have revealed that in the initial structure exhibits an almost null stacking fault probability. However, this does not signify that stacking faults are not present in the initial structure. Indeed, stacking faults can be observed in TEM experiments [15] but their initial presence is rather scarce. The fault probability was shown to increase with plastic deformation. This is clearly shown in the rolling experiment on IGC-synthesized nanocrystalline Pd. Indeed, in Fig. 2.4, presenting the evolution of the stacking fault parameter with strain for an ultrafine grain Pd sample and nanocrystalline Pd sample with grain size ~33 nm, one can clearly see that the stacking fault parameter increases sharply with deformation until it reaches a plateau. The value of the stacking fault parameter is consistently higher in the case of the NC samples. Although this measure is purely qualitative, it reveals an interesting phenomenon. That is, the activity of dislocations is driven by the motion or interaction of Shockley partial dislocations (which necessarily result in the presence of stacking faults). Moreover, it was also suggested that twinning deformation mode may be caused by the stacking faults led by Shockley partial dislocations.

2.1.2 Grain Boundaries

The microstructure of grain boundaries has been subject to a long-lasting debate. Recall that the first studies by Gleiter and co-workers on small-grained nanocrystalline materials, with grain size in the neighborhood of 10 nm, exhibited an *open structure*of grain boundaries which were consequently referred to as anomalous with respect to that of coarse grained materials.

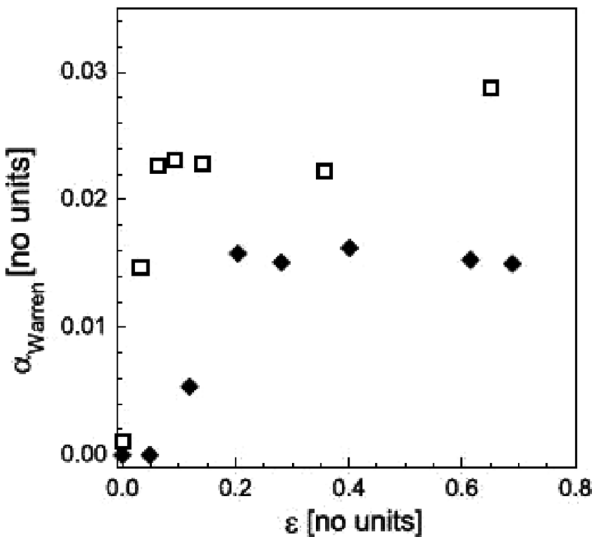

Fig. 2.4 Evolution of the stacking fault parameter with strain for UFG PD (*in bold*) and nanocrystalline IGC Pd

Although this will be described in detail in Chapter 5, let us briefly discuss here the modeling of grain boundaries in coarse-grained polycrystalline materials. Grain boundaries can be regarded as particular groups of geometrically necessary dislocations. Indeed, dislocations can generally be put into two categories: (1) statistically stored dislocations, and (2) geometrically necessary dislocations. Statistical dislocations are present as a consequence of hardening, which results in the decrease of the mean free path of dislocations. Some other dislocations referred to as geometrically necessary must be present within the material in order to accommodate for local lattice curvature changes. Grain boundaries are regions of high change in lattice curvature. Hence, they can be regarded as regions of high density of geometrically necessary dislocations.

First, the grain boundary thickness or width is known not to exhibit major size effects and can be regarded as constant and equal to approximately 3–4 perfect lattice spacing (~0.6–1 nm). Also, grain boundaries are regions of lower atomic density. This leads to the presence of strain fields within the grain cores induced by those within the grain boundaries. A simple model based on the scattering cross-section measurements and neglecting porosity effects leads to an estimate of density for grain boundaries of 60–70% of that of the perfect lattice.

Regarding the detailed microstructure of grain boundaries, two schools are opposed. The first one suggests an open structure of grain boundaries where no atomic order is present while the second school of thought regards grain boundaries as a much more defined phase which in most cases can be described by structural unit models (see Chapter 5). Let us consider the limit

case where the grain size takes the theoretical value zero; in that particular configuration one cannot expect any particular atomic ordering of the "interphase." Now taking the other extreme where a sample would be constructed of simply two grains delimited by a single grain boundary, one would expect a much more organized grain boundary microstructure. In the case of nanocrystalline materials with grain size larger than ~10 nm, so that the triple junction volume fraction does not come into account, one would then expect to find well-defined grain boundary regions, pertaining to the second school of thought, and other interphase regions exhibiting less order. As shown in TEM observations on nanocrystalline Pd with ~10 nm grain size processed by a physical vapor deposition technique, the grain boundary microstructure is not homogeneous within the material. In Fig. 2.5, presenting a HRTEM image of a NC Pd sample processed by physical vapor deposition, some regions, such as region A-B, present a well-ordered grain boundary, while region D-E presents no particular order and region B-C exhibits a grain boundary with changing character. Let us note here that the sample presented has a small grain size, even in the nanocrystalline regime, hence one could probably suppose that an increase in the grain size may lead to more order in the grain boundary region.

As the various fabrication processes differ vastly and due to the limited data on the grain boundary structure, which is inherent to the difficulty in preparing samples for observations, it is rather difficult to discuss grain boundary microstructure in its general sense. However, outstanding observations performed by Huang and co-workers revealed that, in the case of materials processed by severe plastic deformation, both one-step and two-step processes (e.g., HPT, ECAP, and ball milling), grain boundaries are usually high-energy and exhibit strains and steps or curves [13].

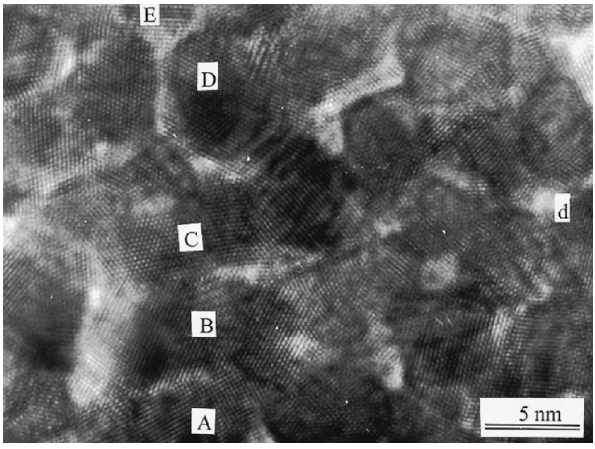

Fig. 2.5 HRTEM image of a nanocrystalline Pd sample. Extracted from [18]

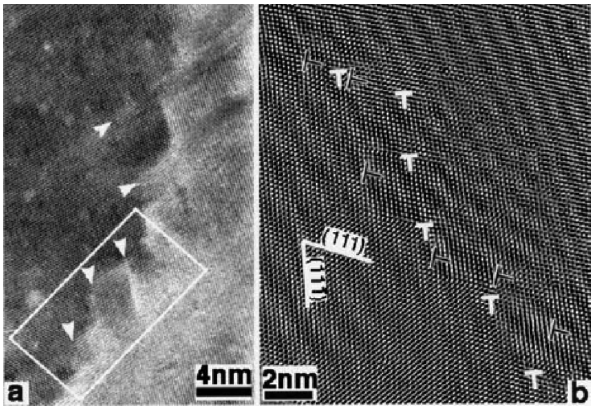

Fig. 2.6 Small angle grain boundary with steps and stacking faults (**a**) and zoom on the selected region revealing the presence of extrinsic stacking faults (**b**) [13]

In Fig. 2.6(a) one can observe a small-angle asymmetric grain boundary with a 2 degree misorientation angle. One can easily observe the presence of strips which are representative of thin twin or stacking faults. Now, looking at Fig. 2.6(b), corresponding to a zoom on the selected window of Fig. 2.6(a), one can observe the presence of slightly disassociated dislocations which are responsible for the presence of the stacking fault or thin twins within the adjacent grain cores. It is thus clear that the grain boundary structure has a great influence on the microstructure of the sample and this influence is not limited to that on the interphase. Finally, let us note that small-angle grain boundaries are known to be dislocation sources operating in a manner similar to that of a traditional Frank and Read source.

As mentioned in Chapter 1, most grain boundaries are large-angle grain boundaries. Similar to the case of small-angle grain boundaries, large-angle grain boundaries typically present facets or steps that correspond to extra-atomic layers. This can be observed in Fig. 2.7 presenting a large-angle grain

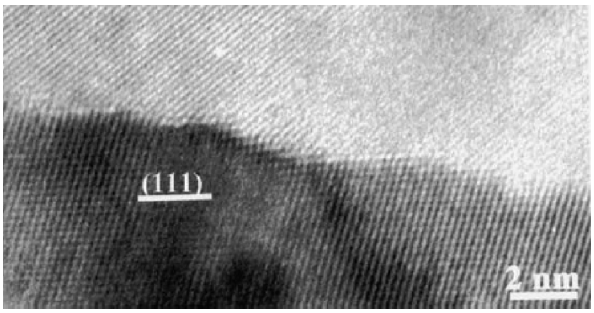

Fig. 2.7 HRTEM image of a high-angle stepped grain boundary in cryomilled Cu [13]

boundary observed in cryomilled Cu. The observed steps are 4–5 atomic layers thick and are lying on the (111) plane. These steps can also be regarded as large ledges. Let us note that in the early 1960s, J.C.M. Li in his pioneering theoretical work, suggested that grain boundary ledges can act as dislocation donors. Hence, upon emitting a dislocation, a grain boundary ledge corresponding to a single layer of extra atoms would be annihilated. As will be shown later, the role of these steps may not be limited to that of dislocation donors.

Most of the defects in nanocrystalline materials are localized within the grain boundaries, which is especially the case of small pores and large flaws that can be as long as one micron. In the case of IGC-processed samples, during the outgassing step followed by warm compaction, it was clearly shown that gas can remain trapped within the pores at pressures high enough to stabilize the pore.

2.1.3 Triple Junctions

Triple junctions are regions where more than two grains meet. Considering the fact that the atomic positions in a grain boundary are directly dependent on the relative five degrees of freedom of the two grains composing the grain boundary resulting in a particular spatial organization of the atoms, it is expected that the position of atoms localized within a triple junction will clearly depend on the relative orientation of the neighboring grains. TEM observations revealed that no regular organization of the atoms can be observed in a triple junction. This can be clearly observed in region denoted *d* in Fig. 2.5. Also, as in the case of grain boundaries, triple junctions are regions of concentrated defects such as pores, flaws, and impurities.

2.2 Mechanical Properties

Nanocrystalline materials exhibit fascinating properties which are intimately linked to their particular microstructure characterized by a large volume fraction of grain boundaries. One of the most acknowledged and studied peculiarities of nanocrystalline materials is the extremely high yield strength that can be reached with small grain size. Indeed, a typical NC sample will exhibit yield strength up to 7 times larger than its coarse grain counterpart with the same composition.

Let us recall that when decreasing the crystallite size to the nanorange, one hopes to reach a great if not an optimal compromise between strength and ductility. This has not yet been reached, but giant steps were taken in that direction over the past decade. More than the grain size/yield strength dependence, nanocrystalline materials exhibit other size-dependent properties. Some are expected, such as the size-dependent elastic constants and others needing detailed modeling. This is the case of the strain rate sensitivity discussed below.

Also, as nanosized particles exhibit poor thermal stability and since grain boundaries in nanocrystalline materials are typically high-energy grain boundaries, a particular size effect in the thermal response of nanocrystalline materials is expected. This particular subject still requires a great deal of investigation to understand the underlying phenomenon.

A word of caution is necessary when analyzing experimental data on nanocrystalline materials. First, as will be presented below, most available data exhibit large discrepancies. This has unfortunately lead to a great deal of debate among modelers. Hence, prior to analyzing data on the mechanical or thermal response of a sample, it is crucial to cautiously analyze the fabrication process and resulting microstructure. Indeed, as shown in Chapter 1, the sample microstructure is a direct consequence on the fabrication process which so far is particular for each, mostly academic, laboratory. Second, the measurement of several properties of NC materials is rather complicated. Let us cite two stringent examples.

Typically, the yield stress of a sample is measured by tensile test and subsequent application of the 0.2% offset rule. However, in the case of NC materials, the samples are typically of reduced dimensions and it is not always possible to perform a tensile test on the samples. Hence, nanohardness measurements are often performed and the yield stress is simply deduced by dividing the hardness by 3. This is a commonly acceptable approximation in the case of coarse grain materials. However, it has been reported that, in the case of NC materials, hardness measurements consistently lead to higher values of the yield strength than obtained by tensile tests. Moreover, hardness measurements are very inhomogeneous within the material. Also, as can be observed in Fig. 2.8, the effect of artifacts such as porosity is far from being negligible. Indeed, one can see that powder compacts with densities lower than 99.5% exhibit hardness on the order of 30% lower than samples with higher density.

Second, let us take the example of the estimation of the grain size. The two most frequently used methods are (1) observation via TEM experiments and

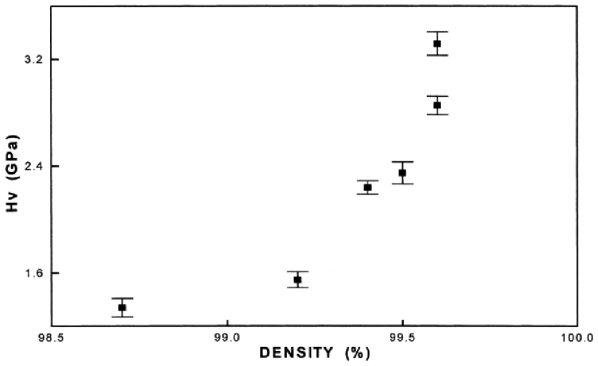

Fig. 2.8 Hardness versus density of the powder compact. Extracted from [19]

(2) XRD measurements combined with the use of the Scherrer formula. The first method consists of preparing a thin sample for observation in a transmission electron microscope. Although the sample preparation is rather delicate, ion milling is an effective method of preparation. Then, the grain size is measured on a given number of grains. Note that the number of grains observed must be sufficient for the estimated grain size to be representative of the actual mean grain size of the sample. Also, different regions of the sample must be selected because the grain size may be highly inhomogeneous within the material. Finally, the grain shape, which is certainly not ideally spherical, adds to the difficulty of mean grain size estimation. The second method consists of preparing a sample for XRD analysis and using the well-known Scherrer formula given by [20, 21]:

$$d = \frac{K\lambda}{B\cos\theta} \tag{2.2}$$

Here, K is the Scherrer constant, λ the X-ray wavelength, *B*is the integral breadth of a reflection located at 2θ. Grain size measurement from XRD and TEM observations rarely leads to the same predictions. Let us note, however, that the two measures remain in the same ballpark. However, for modeling purposes precise values are often required. Keeping in mind this word of caution, let us now present the mechanical and thermal response/properties of nanocrystalline materials.

2.2.1 Elastic Properties

The elastic response of a material is directly correlated to the interatomic bonds within the sample and on atomic structure/ordering. Since the volume fraction of interphase (e.g., triple junctions and grain boundaries) can increase up to 10-fold in the case of nanocrystalline materials compared to that of coarse-grain materials, and since grain boundaries exhibit a structure different from the perfect crystal lattice, it is natural to expect a size effect in the elastic response of nanocrystalline materials. Also, due to the fact that the grain boundary density is smaller than that of a perfect crystal, revealing a more *open structure*, one expects a decrease in the elastic constants of nanocrystalline materials. This can be observed in Fig. 2.9, presenting experimental measures from several different teams, of the Young's modulus of pure Cu sample as a function of grain size. Indeed, one can notice that for grain size smaller than 40 nm, corresponding to a volume fraction of interphase larger than ~10%, a decrease in Young's modulus ranging from ~6 to ~30% is exhibited by NC materials. However, let us note that some of the lower values are likely to be biased by poor consolidation.

Fig. 2.9 Experimental measurements of Young's modulus as a function of grain size

2.2.1.1 Yield Stress

Coarse grain polycrystalline metals are known to exhibit a size-dependent yield stress obeying the Hall-Petch law [22, 23]. It predicts an increase in the yield stress proportional to the inverse of the square root of the grain size and is given by:

$$\sigma_y = \sigma_0 + \frac{K_{HP}}{\sqrt{d}} \tag{2.3}$$

Here, σ_0 is the friction stress, σ_y is the yield strength of the material, K_{HP} is the Hall-Petch slope, and d is the grain size. Modeling of the Hall-Petch law has been subject to intensive studies over the past decades. All models are based on the dislocation-dislocation interaction. First, models based on the pile-up of dislocations localized at the grain boundaries were developed [23]. However, body-centered cubic materials, in which dislocation pile-ups do not occur, are known to respect the Hall-Petch law. Second, J.C.M. Li proposed a model accounting for the Hall-Petch law based on the emission of dislocations by grain boundary ledges [24]. In Li's model, a dislocation emitted from a grain boundary ledge, corresponding to a step or extra atomic layer localized at the grain boundary, will interact with a dislocation forest in the vicinity of the grain boundary. The dislocation density within the forest is then related to the grain boundary misfit angle, which is itself dependent on the grain boundary ledge density. Murr and Venkatesh dedicated substantial time and effort in showing a dependence of the yield strength on the grain boundary ledge density as predicted in Li's theoretical work [25–28]. Although the ledge density affects the yield stress of the material, it was also shown that with the fabrication processes used then, the ledge density decreased with grain size. Hence, Li's theory was

shown to need further refinement. Finally, models based on the strain gradient engendered by the presence of geometrically necessary dislocations were also successful in modeling the Hall-Petch law [29, 30].

The appeal of the Hall-Petch law is evident. Let us consider the case of pure copper, which typically exhibits a Hall-Petch slope of $0.11\, MPa \cdot \sqrt{m}$. Starting from a 1 μ grain size material with 180 Mpa yield stress, and decrease the grain size to. say. 50 nm, according to the Hall-Petch law, the yield stress of the fine-grained copper sample will be 561 MPa. In other words, the yield strength is multiplied by a factor of 3.

Recall that when the grain size is decreased to the nanorange, experiments on nanocrystalline samples produced by various fabrication processes have revealed that below a critical grain size, the yield stress deviates from the Hall-Petch law. Precisely, the critical grain size is $d_c \approx 25\, nm$ and below d_c the Hall-Petch slope can either decrease or even become negative.

A limited number of data are available to precisely describe the breakdown of the Hall-Petch law and, as mentioned in the beginning of this section, most available data are inconsistent due to (1) the different type of measurements methods (e.g., tensile tests, compressive tests, hardness measurements) and (2) the presence of artifacts within the samples. Indeed, due to poor particle bonding the yield stress and maximum elongation of nanocrystalline samples differs largely in compression tests and in tensile tests. Figure 2.6 presents the experimental measurements of the yield stress with the inverse of the square root of the grain size. Although the data presented in Fig. 2.10 exhibit noticeable scatter, one can clearly observe a deviation from the Hall-Petch law (represented by the dashed line). Let us note that to be consistent a measure of the size effect in the yield stress shall be performed with a single fabrication process allowing variation of the sole grain size parameter.

The breakdown of the Hall-Petch law has been subject to vigorous debate. This is easily understandable by looking at Fig. 2.10. Indeed, since most nanocrystalline samples present artifacts it is rather delicate to impede the observed breakdown of the Hall-Petch law as an intrinsic characteristic of nanocrystalline materials or as resulting from the previously mentioned defects. Moreover, thanks to a better control on the processing routes, the quality of samples has tremendously improved over the past decade and the critical grain size has continuously decreased. However, with consistent and meticulous modeling, a general agreement as to the fact/artifact breakdown of the Hall-Petch law was reached.

Currently, the general consensus on the evolution of yield stress with grain size is the following (see Fig. 2.11). In the case of polycrystalline materials with grain size ranging from several microns down to ~100 nm, the Hall-Petch law is respected. When the grain size ranges from ~100 nm down to ~25 nm a decrease in the Hall-Petch slope is expected. However, the slope is expected to remain positive. Finally, a negative Hall-Petch slope is expected when the grain size is smaller than a critical grain size that is believed to be in the neighborhood of ~10 nm. Hence, this suggests that experiments showing a breakdown of the

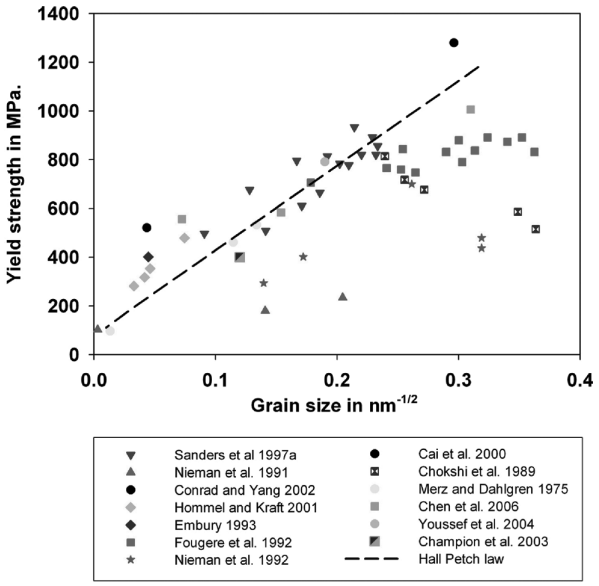

Fig. 2.10 Experimental data presenting yield stress as the function of the inverse of the square root of the grain size

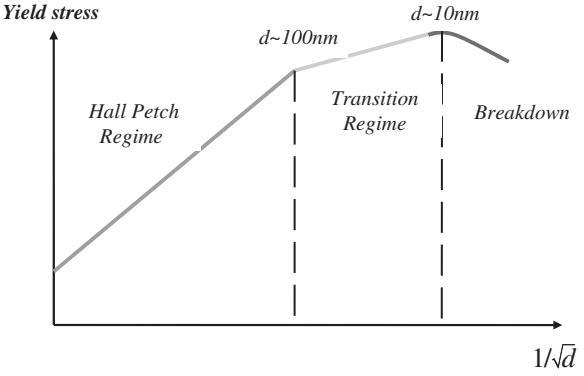

Fig. 2.11 Plot of the expected grain size dependence of yield stress for ideal samples

Hall-Petch law occurring at a critical grain size in the order of ~25 nm may be hindered by artifacts such as poor particle bonding or contamination.

2.2.2 Inelastic Response

2.2.2.1 Ductility

Due to poor sample quality, the first samples exhibited limited ductility with maximum elongation rarely exhibiting 2–3%, and the few samples exhibiting

larger maximum deformation did not reach the expected yield strength. Hence, the capability of nanocrystalline materials to exhibit a ductile behavior was severely questioned [31]. However, with the progress in fabrication processes and particularly in consolidation of nanocrystalline powders, samples with narrow grain size distributions and bimodal distribution exhibited relatively large ductility and extremely high yield strength [31–38]. This is shown in Fig. 2.12 presenting the yield strength of Cu samples as a function of maximum elongation from various sources (date, fabrication process, and grain sizes are presented in the legend). One can easily judge the tremendous progress made over the past decade. While first samples exhibited 2–3% ductility, the most recent samples are now capable of deforming up to 50% with much higher yield strength than coarse grain materials. The latter were fabricated by ball milling in an inert gas environment and graphite plates were placed in the compression dies to ensure no sample contamination.

As shown in Fig. 2.12, the early NC samples typically exhibited limited ductility. Indeed, most samples typically exhibit a maximum elongation smaller than 5% deformation. This has been one of the most limiting factors preventing industrial applications of NC materials as structural materials. The limited ductility of these NC samples is rather abnormal in the case of coarse-grained materials; a grain refinement typically results in an enhanced ductility of the materials. Indeed, a microcrack has more chance of being stopped by a barrier – such as a grain boundary – in more refined samples. The presence of defects in the as processed samples naturally impacts the ductility of NC materials. For example, one would expect electrodeposited samples containing residues such as S and O atoms to exhibit a borderline brittle behavior. This can be seen in NC Ni samples produced by electrodeposition, which exhibit close to no plastic response prior to failure (see the TEM image presented in Fig. 2.13) [39].

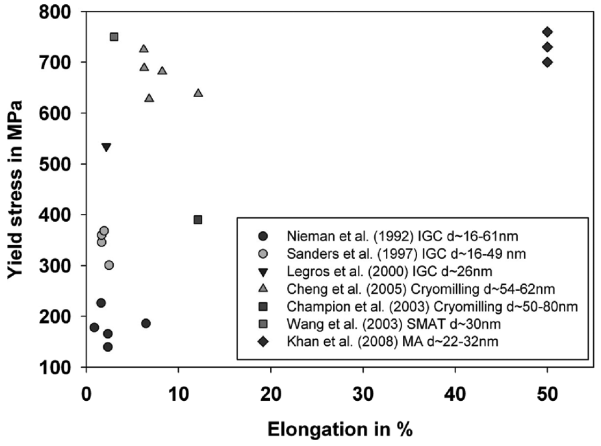

Fig. 2.12 Experimental data presenting a yield strength vs. elongation plot

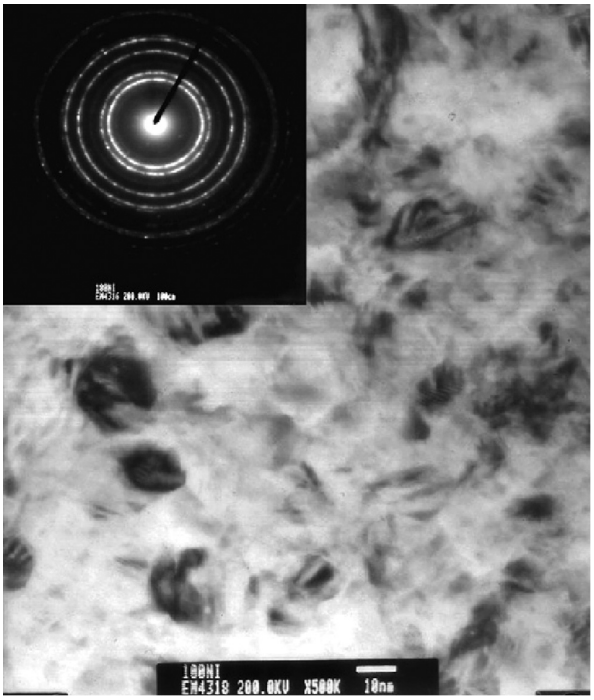

Fig. 2.13 TEM image of a NC electrodeposited Ni samples deformed in tension

Clearly, the superior ductility of the samples of Khan et al. results from the high purity resulting from meticulous sample preparation.

2.2.2.2 Flow Stress

Active plastic deformation mechanisms in NC materials are expected to differ from that of coarse-grain materials. This is due to the fact that the dislocation density, activity, and grain boundary volume fraction largely differ in these two classes of materials. Moreover, mechanisms that are not expected to be active at room temperature and in the quasi-static range are suggested to participate to the deformation of NC materials. This is the case of grain boundary sliding and deformation twinning, for example.

NC materials exhibit particular inelastic response that is often qualified as quasi or almost elastic perfect plastic. This is shown in Fig. 2.14, presenting a true stress vs. true strain curve of a NC Cu sample with 50 nm grain size and of coarse-grain Cu sample. It can clearly be seen that while the coarse grain sample exhibits significant strain hardening – engendered by dislocation activity – the NC sample exhibits a near-perfect elastic plastic response. The plastic response can be decomposed into three regions: (1) work hardening domain with

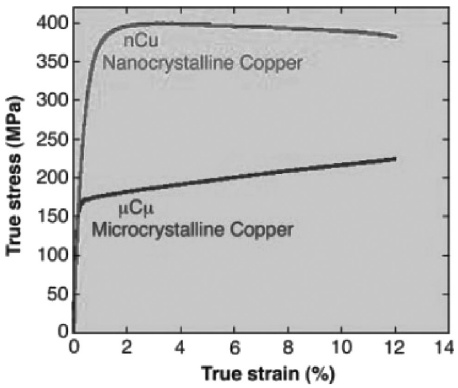

Fig. 2.14 Experimental true stress true strain curve of nanocrystalline Cu with 50 nm grain size and coarse grain Cu [34]

decreasing strain exponent towards zero, (2) plastic yielding domain at constant flow stress, and (3) plastic yielded with linear softening. This reinforces the idea that the active plastic deformation mechanisms in NC materials differ from those in coarse-grain polycrystalline materials.

2.2.2.3 Strain Rate Sensitivity

In the thermal activation regime, the behavior of metallic materials is often phenomenologically can be described with use of a power law (e.g., $\dot{\varepsilon} = \dot{\varepsilon}_0(\sigma/\sigma_{critt})^{1/m}$, the inverse of this law is also used), which is an approximation of exponential laws, accounting for the thermally activated nature of the deformation mechanisms. A well-known example is that of the description of the effect of dislocation glide [11]. The exponent m, used in power laws, is referred to as the strain rate sensitivity and typically considered constant during deformation in continuum models. In fact, the strain rate sensitivity parameter varies slightly during deformation (due to the change in activation volume and flow stress).

Let us recall that the strain rate sensitivity is typically used to determine active plastic deformation mechanism. For example, $m = 1$ typically corresponds to the activity of Coble creep, that is the steady state vacancy diffusion along the grain core/grain boundary interface. Similarly, $m = 0.5$ suggests the activation of grain boundary sliding. Hence, a change in hardening coefficient is an element suggesting a change in the nature of the dominant plastic deformation process. It is usually given by:

$$m = \frac{\sqrt{3}kT}{v\sigma} \tag{2.4}$$

Here, k, T, ν, and σ refer to the Boltzmann constant, the absolute temperature, the activation volume, and the uniaxial tensile stress. Note here that depending on the expression of the power law, some authors define *m* as the inverse of the present definition.

Strain rate jump experiments performed on several NC samples have clearly shown an increase in the strain rate sensitivity compared to that of their coarse grain counterparts. For example, Cheng and co-workers report a value of 0.027 for 62 nm grain Cu while *m* is typically equal to 0.006 in coarse-grain Cu [31]. Numerous experiments have confirmed the increase in strain rate sensitivity with decreasing grain size [40]. Figure 2.15 presents literature data showing the evolution of the strain rate sensitivity as a function of grain size [7, 31, 35, 40, 41]. An obvious increase in the strain rate sensitivity parameter with a decrease in grain size can be observed. It has been suggested in a relatively large number of models that the grain size dependence of the strain rate sensitivity parameter results from a decrease in the activation volume [31, 41].

2.2.2.4 Thermal Stability

Nanocrystalline materials exhibit abnormal thermal stability characterized by rapid grain growth at temperatures above a critical value (which is obviously dependent on the material considered). This issue avers to be critical for – as discussed in previous chapter dedicated to fabrication processes – the synthesis of NC materials may require temperature treatment. For example, this would be the case of a sample fabricated with a two-step process. Therefore, it is relatively difficult to retain the nanofeatures of the material during its fabrication. Moreover, the abnormal temperature stability of NC materials also impedes their use in the industry. Indeed, as the grain size of the material increases, its response will change – and more than likely deteriorate for the particular application considered.

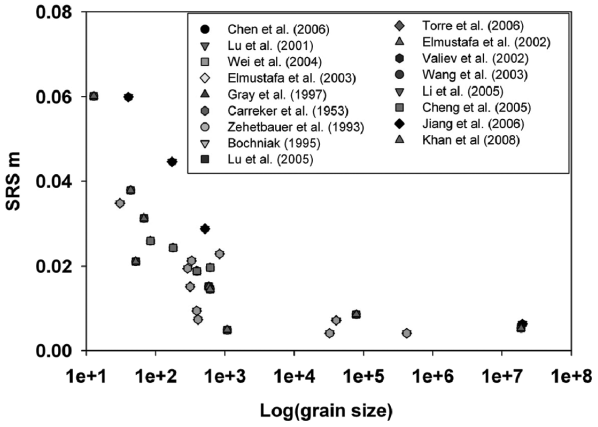

Fig. 2.15 Strain rate sensitivity parameter as a function of grain size. Extracted from [41]

Grain growth in conventional polycrystals can be either homogeneous – in the sense that the grain size distribution remains rather uniform – or not. In the former case, the evolution of grain growth with annealing time (at constant temperature) is given empirically by a parabolic law of the following form [42]:

$$d^{1/n} - d_0^{1/n} = kt \tag{2.5}$$

Here, d and d_0 denote the instantaneous grain size and the initial grain size, respectively. $t$denotes the time and k is the temperature-dependent grain growth constant. The rate of growth exponent is typically equal to 2. However, some deviations have been observed. Also, grain growth is typically initiated at $0.5\,T/T_m$(T_m denotes the melting temperature). Typically, the grain growth constant is related to the grain boundary mobility. For example, this is the case in Hillerts' model based on the idea – generally accepted – that the grain boundary mobility is proportional to the pressure difference resulting from its curvature [42]. As discussed in work by Lu, one would expect the thermal instability of a polycrystals – characterized by the smallest temperature at which grain growth sets off – to decrease as the grain size decreases. However, this is not necessarily the case for nanocrystalline materials which typically exhibit an higher than expected critical temperature. For example, 20 nm NC aluminum prepared by mechanical attrition exhibit a stable grain size until $0.72\,T/T_m$ [43]. Several explanations have been proposed to explain such a phenomenon. For example, the grain boundary mobility may be decreased in NC materials due to solid impurities causing drag. Generally, the following abnormal thermal effects are found to occur in NC materials:

- The starting temperature, the peak temperature and the activation energy increase with decreasing grain size.
- Discontinuous grain growth occurs at a critical temperature. At this critical temperature, the rate of grain growth increases drastically. This can be seen in annealing experiments by Song et al. [44]. Figure 2.16a presents the

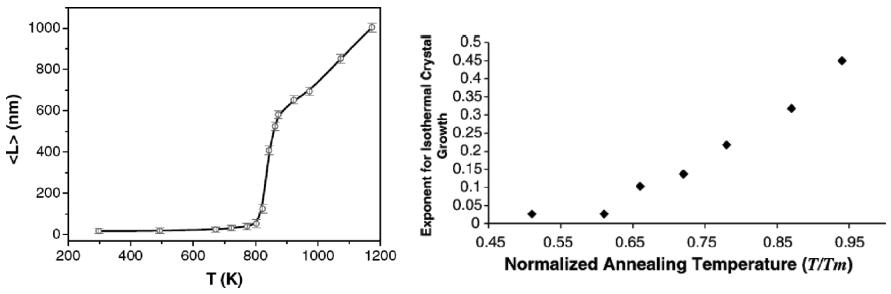

Fig. 2.16 (**a**) Evolution of mean grain size as a function of annealing temperature (pure nanocrystalline Co), extracted from [44]; (**b**) best fit growth exponent as a function of annealing temperature [43]

evolution of the mean grain size of a pure NC Co sample subjected to 1 h annealing as a function of annealing temperature.

- The grain growth exponent – chosen for each annealing temperature to obtain a best fit of the average grain size vs. annealing time curve – increases with the normalized annealing temperature to reach a value close to the typical ½ value for conventional metals [43]. This can be observed in Fig. 2.12.b presenting the evolution of the growth exponent as function of annealing temperature for NC Al samples.
- During an annealing experiment at a given constant temperature, the evolution of the average grain size as a function of time is characterized by a change in the grain growth exponent. Precisely, the growth rate decreases monotonically with time.

Several models were developed to rationalize the four points mentioned in the above. Some of the most acknowledged models are that of Fecht [45] and Wagner [46]. Both models establish thermal properties of grain boundaries based on the idea (which is yet to be shown experimentally) that grain boundaries present an excess volume compared to a perfect crystal. Recently, Song et al. [44] introduced a model combining the two approaches used by Fecht and Wagner and proposed a convincing explanation of the abnormal thermal effects in NC materials. For the sake of comprehension, the aforementioned model will be described in what follows. First, if V denotes the grain boundary atomic volume and V_0 denotes the atomic volume of a perfect crystal, the excess volume of grain boundaries can be expressed as follows:

$$\Delta V = \frac{V}{V_0} - 1 \tag{2.6}$$

This excess volume is thought to decrease with an increase in the grain size. Therefore, as the grain size is decreased the volume fraction of grain boundaries increases – this was seen previously – as well as the excess volume of grain boundaries. Assuming the thermal features of grain boundaries to be similar to that of a dilated crystal, a universal equation of state and the quasi-harmonic Debye approximation are combined to predict the evolution of the excess enthalpy, excess entropy, and excess free energy as a function of the excess volume. The quantity of interest here is the excess free energy which is predicted to evolve as shown in Fig. 2.17.

In agreement with experiments (see Fig. 2.16), it is predicted that there is a critical excess volume ΔV_c – and consequently a critical grain size – at which the discontinuous grain growth occurs. When the excess volume is larger than the critical excess volume (e.g., the grain size is smaller than a critical value), the excess free energy is smaller than the maximum value and the material is in a more stable state than at smaller excess volumes (e.g., larger grain size). The converse reasoning is also true. When the excess volume is equal to the critical

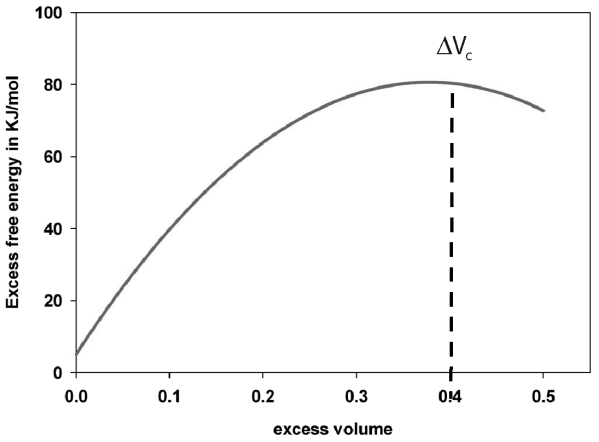

Fig. 2.17 Schematic of the evolution of the excess free energy of grain boundaries with excess free volume

value, the system is not thermally stable and thermal activation alone could destabilize the system. Therefore, one expects to observe a critical temperature at which the rate of grain growth changes abruptly.

An effective stabilization method consists of adding impurities or dopants to a pure mixture. For example, nanocrystalline Al was prepared by mechanical attrition in both a nylon and a stainless steel media. Mechanical attrition in the nylon media is clearly expected to lead to impurities within the sample. The onset of grain growth occurred at $0.72\,T/T_m$ and $0.83\,T/T_m$ in the stainless steel and nylon media, respectively. Indeed, the addition of dopants is expected to decrease excess free energy of grain boundaries. This was already predicted in Gibbs pioneering work where the evolution of the grain boundary energy, γ, evolves with the dopant coverage (that is the amount of dopant in the grain boundary), Γ, and its chemical potential, μ, as follows [47]:

$$d\gamma = -\Gamma\, d\mu$$

Recent molecular simulations – using the isothermal-isobaric (NPT) ensemble (see Chapter 4) – on high-angle bicrystal interfaces have shown the effect of the amount of dopant and its radius on the grain boundary energy. Such effects are shown in Fig. 2.18 [48]. It can be seen that a decrease in the dopant radius leads to a decrease in the grain boundary energy. Similarly, an increase in the dopant coverage leads to a decrease in the grain boundary excess energy. Interestingly, Fig. 2.18 suggests that there is a critical dopant coverage – such that the excess free energy of grain boundaries is null – (function of the dopant radius) which would stabilize grain boundaries.

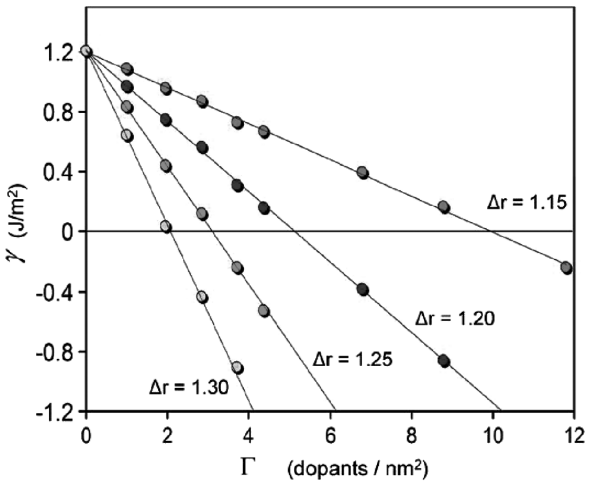

Fig. 2.18 Grain boundary energy as a function of dopant segregation for several dopant radii. Extracted from [48]

2.3 Summary

Nanocrystalline materials exhibit a particular microstructure characterized by a large volume fraction of grain boundaries and triple junctions. Nanosized grain cores retain a crystalline structure presenting lattice strains. Triple junctions present a structure devoid of regular organization while the structure of grain boundaries can exhibit changing character. Grain boundaries typically present an excess volume. Most fabrication processes lead to high large-angle grain-boundary contents.

NC materials exhibit several peculiarities. First, the evolution of yield stress with grain size does not respect the Hall-Petch law. Below a critical grain size d $\sim$20 nm the yield stress decreases with decreasing grain sizes.

Second, the quasistatic response of NC materials largely differs from that of coarse-grain materials. Indeed, the strain rate sensitivity of NC materials is higher than that of coarse grain polycrystalline materials. Also, while coarse grain materials exhibit strain hardening, NC materials exhibit a pseudo-elastic perfect plastic response.

Third, the ductility of NC materials was shown to be severely affected by the materials' purity. However, ductility can be improved by tailoring the grain size distribution. High-purity, bimodal grain size distributions, and wide distributions lead to larger elongation to failure.

Finally, the thermal response of NC materials is characterized by a regime of rapid grain growth at a critical temperature. The latter depend on the material processed. This can be prevented by adding dopants to the sample during fabrication.

References

1. Champion, Y. and M.J. Hytch, The European Journal of Applied Physics **4**, (1998)
2. Palumbo, G., S.J. Thorpe, and K.T. Aust, Scripta Metallurigica et Materialia **24**, (1990)
3. Birringer, R., Materials Science and Engineering A **117**, (1989)
4. Zhang, K., I.V. Alexandrov, and K. Lu. *The X-ray diffraction study on a nanocrystalline Cu processed by equal-channel angular pressing*. Kona, HI, USA: Elsevier, (1997)
5. Kumar, K.S., S. Suresh, M.F. Chislom, J.A. Horton, and P. Wang, Acta Materialia **51**, (2003)
6. Straub, W.M., T. Gessman, W. Sigle, F. Phillipp, A. Seeger, and H.E. Schaefer, Nanostructured Materials **6**, (1995)
7. Torre, F.D., P. Spatig, R. Schaublin, and M. Victoria, Acta Materialia **53**, (2005)
8. Ungar, T., S. Ott, P.G. Sanders, A. Borbely, and J.R. Weertman, Acta Materialia **46**, (1998)
9. Estrin, Y. and H. Mecking, Acta Metallurgica **32**, (1984)
10. Kocks, U.F., Transactions of the ASME (1976)
11. Kocks, U.F. and H. Mecking, Progress in Materials Science **48**, (2003)
12. Mecking, H. and U.F. Kocks, Acta Metallurgica **29**, (1981)
13. Huang, J.Y., X.Z. Liao, and Y.T. Zhu, Philosophical Magazine **83**, (2003)
14. Sanders, P.G., A.B. Witney, J.R. Weertman, R.Z. Valiev, and R.W. Siegel, Journal of Engineering and Applied Science **A204**, (1995)
15. Mingwei, C., M. En, K.J. Hemker, S. Hongwei, W. Yinmin, and C. Xuemei, Science **300**, (2003)
16. Markmann, J., et al., Scripta Materialia **49**, (2003)
17. Liao, X.Z., F. Zhou, E.J. Lavernia, D.W. He, and Y.T. Zhu, Applied Physics Letters **83**, (2003)
18. Ranganathan, S., R. Divakar, and V.S. Raghunathan, Scripta Materialia **27**, (2000)
19. Sun, X., R. Reglero, X. Sun, and M.J. Yacaman, Materials Chemistry and Physics **63**, (2000)
20. Patterson, A.L., Physical Review **56**, (1939)
21. Scherrer, P., Gottinger Nachrichten **2**, (1918)
22. Hall, E.O., Proceedings of the Physical Society of London **B64**, (1951)
23. Petch, N.J., Journal of Iron Steel Institute **174**, (1953)
24. Li, J.C.M., Transactions of the Metallurgical Society of AIME **227**, (1963)
25. Murr, L.E., Materials Science and Engineering **51**, (1981)
26. Murr, L.E. and E. Venkatesh, Metallography **11**, (1978)
27. Venkatesh, E.S. and L.E. Murr, Scripta Metallurgica **10**, (1976)
28. Venkatesh, E.S. and L.E. Murr, Materials Science and Engineering **33**, (1978)
29. Ashby, M.F., Philosophical Magazine **21**, (1970)
30. Cheong, K.S. and E.P. Busso, Discrete dislocation density modelling of single phase FCC polycrystal aggregates. Acta Materialia, **52(19)**, 5665–5675, (2004)
31. Cheng, S., et al., Acta Materialia **53**, (2005)
32. Yinmin, W., C. Mingwei, Z. Fenghua, and M. En, Nature **419**, (2002)
33. Youssef, K.M., R.O. Scattergood, K.L. Murty, and C.C. Koch, Applied Physics Letters **85**, (2004)
34. Champion, Y., C. Langlois, S. Guerin-Mailly, P. Langlois, J.L. Bonnentien, and M.J. Hytch, Science **300**, (2003)
35. Khan, A.S., B. Farrokh, and L. Takacs, Materials Science and Engineering: A **489**, (2008)
36. Legros, M., B.R. Elliott, M.N. Rittner, J.R. Weertman, and K.J. Hemker, Philosophical Magazine A: Physics of Condensed Matter, Structure, Defects and Mechanical Properties **80**, (2000)
37. Nieman, G.W., J.R. Weertman, and R.W. Siegel. *Mechanical behaviour of nanocrystalline Cu, Pd and Ag samples*. New Orleans, LA, USA: TMS – Miner. Metals & Amp; Mater. Soc., (1991)

38. Sanders, P.G., J.A. Eastman, and J.R. Weertman, Acta Materialia **45**, (1997)
39. Yim, T., S. Yoon, and H. Kim, Materials Science & Engineering. A, Structural materials **449–451**, (2007)
40. Chen, J., L. Lu, and K. Lu, Scripta Materialia **54**, (2006)
41. Asaro, R.J. and S. Suresh, Acta Materialia **53**, (2005)
42. Hillert, M., Acta Metallurgica **13**, (1964)
43. De Castro, C.L. and B.S. Mitchell, Materials Science and Engineering A **396**, (2005)
44. Song, X., J. Zhang, L. Li, K. Yang, and G. Liu, Acta Materialia **54**, (2006)
45. Fecht, H.J., Physical Review Letters **65**, (1990)
46. Wagner, M., Physical Review B (Condensed Matter) **45**, (1992)
47. Gibbs, J.W., *The collected works*. Green and Co, New York, (1928)
48. Millet, P.C., R.P. Selvam, and A. Saxena, Acta Materialia **55**, (2007)

http://www.springer.com/978-0-387-46765-8

Atomistic and Continuum Modeling of Nanocrystalline Materials
Deformation Mechanisms and Scale Transition
Capolungo, L.
2009, XX, 480 p. 103 illus., Hardcover
ISBN: 978-0-387-46765-8